Mueller matrix decomposition for extraction of individual polarization parameters from complex turbid media exhibiting multiple scattering, optical activity, and linear birefringence

Nirmalya Ghosh
Michael F. G. Wood
Ontario Cancer Institute
Division of Biophysics and Bioimaging
University Health Network
    and
University of Toronto
Department of Medical Biophysics
610 University Avenue
Toronto, Ontario, Canada M5G 2M9

I. Alex Vitkin
Ontario Cancer Institute
Division of Biophysics and Bioimaging
University Health Network
    and
University of Toronto
Department of Medical Biophysics and Radiation
    Oncology
610 University Avenue
Toronto, Ontario, Canada M5G 2M9

Abstract. Linear birefringence and optical activity are two common optical polarization effects present in biological tissue, and determination of these properties has useful biomedical applications. However, measurement and unique interpretation of these parameters in tissue is hindered by strong multiple scattering effects and by the fact that these and other polarization effects are often present simultaneously. We have investigated the efficacy of a Mueller matrix decomposition methodology to extract the individual intrinsic polarimetry characteristics (linear retardance δ and optical rotation ψ, in particular) from a multiply scattering medium exhibiting simultaneous linear birefringence and optical activity. In the experimental studies, a photoelastic modulation polarimeter was used to record Mueller matrices from polyacrylamide phantoms having strain-induced birefringence, sucrose-induced optical activity, and polystyrene microspheres–induced scattering. Decomposition of the Mueller matrices recorded in the forward detection geometry from these phantoms with controlled polarization properties yielded reasonable estimates for δ and ψ parameters. The confounding effects of scattering, the propagation path of multiple scattered photons, and detection geometry on the estimated values for δ and ψ were further investigated using polarization-sensitive Monte Carlo simulations. The results show that in the forward detection geometry, the effects of scattering induced linear retardance and diattenuation are weak, and the decomposition of the Mueller matrix can retrieve the intrinsic values for δ and ψ with reasonable accuracy. The ability of this approach to extract the individual intrinsic polarimetry characteristics should prove valuable in diagnostic photomedicine, for example, in quantifying the small optical rotations due to the presence of glucose in tissue and for monitoring changes in tissue birefringence as a signature of tissue abnormality. © *2008 Society of Photo-Optical Instrumentation Engineers.* [DOI: 10.1117/1.2960934]

1 Introduction

The use of polarimetric techniques has received considerable recent attention for biomedical diagnosis.[1] This is because the polarization properties of scattered light contain additional diagnostic information on tissue, which cannot be obtained from the use of unpolarized light. For example, collagen (a structural protein) and other fibrous tissues exhibit linear birefringence due to their oriented structures. In various kinds of tissue abnormalities, the structural (and functional) properties of collagen and other fibrous structures show distinct changes. Measurement of the linear birefringence of tissue may thus find useful applications in noninvasive diagnosis of various pathological diseases.[2–5] Glucose is another important tissue constituent that possesses circular birefringence due to its asymmetric chiral structure. Its presence in tissue leads to rotation of the plane of linearly polarized light about the axis of propagation (known as optical rotation). Measurements of optical rotation may offer an attractive approach for noninvasive monitoring of tissue glucose levels, and several studies

Address all correspondenc to Alex Vitkin, Dept. of Medical Biophysics and Radiation Oncology, University of Toronto, 610 University Avenue, Toronto, Ontario, Canada M5G, 2M9. Tel: +1-416-946-2990; Fax: +1-416-946-6529; E-mail: vitkin@uhnres.utoronto.ca

have investigated the polarization properties of scattered light from chiral turbid medium.[6–16] In addition to these applications, polarimetric measurements are also finding use for contrast enhancement in biomedical imaging.[17–21]

The use of the polarimetric techniques for biological tissue characterization is, however, severely hampered by multiple scattering effects. In a turbid medium such as tissue, the incident polarized light becomes strongly depolarized due to multiple scattering, the magnitude and rate of depolarization being determined by a large number of parameters such as the concentration, size, shape, refractive index of the scatterers, detection geometry, and by the incident light's state of polarization.[22–25] Polarization modulation and synchronous detection methods, therefore, have been developed to extract the weak fraction of the polarization preserving component of scattered light from a turbid medium and analyze it for determination of the diagnostically relevant polarization properties such as linear birefringence and optical activity.[7,9,10,26] In particular, this approach is being investigated to determine of the concentration of optically active glucose in human tissue. However, studies have shown that even when depolarization due to multiple scattering is taken into account, the relatively small rotation of the polarization vector arising from optical activity in the medium is hidden by the much larger change in the orientation angle of the polarization vector due to scattering.[7,27] In addition to the scattering effects, interpretation of optical rotation using the conventional Stokes polarimetry-based approach is further confounded by the effects of linear birefringence and its complex orientation in real tissues.

Because the Mueller matrix (which transforms the Stokes vector describing the polarization properties of incident light to the Stokes vector of scattered light) description contains complete information about all the polarization properties of a medium,[28,29] measurements of full Mueller matrix elements may be used to address these issues. However, when many optical polarization effects are simultaneously occurring in the sample (as is the case for tissue), the resulting elements of the Mueller matrix reflect several "lumped" effects, thus hindering their unique interpretation. A methodology that allows the extraction of the individual "intrinsic" material polarimetry characteristics from the lumped Mueller matrix description is thus needed. The independent constituent polarization parameters—linear retardance (δ, difference in phase between two orthogonal linear polarization, and its orientation angle θ), circular retardance or optical rotation (ψ, difference in phase between right and left circularly polarized light), diattenuation (d, differential attenuation of orthogonal polarizations for both linear and circular polarization states), and depolarization coefficient (Δ, linear and circular)—can be efficiently extracted by decomposing the measured Mueller matrix into the "basis" Mueller matrices of a retarder, diattenuator, and depolarizer.[30] The individual polarization parameters obtained through this process should provide more intrinsic information on the underlying morphological features and physiological state of tissue and may thus offer a more fundamental (less empirical) way to understand its structure and behavior.

Indeed, preliminary studies have shown that Mueller matrix decomposition can be used to extract the pure optical rotation component corresponding to the concentration of chiral substances by decoupling the contribution of scattering-induced rotation of the polarization vector that primarily arises due to the contribution of singly (or weakly) scattered photons in a scattering medium.[31] In a highly scattering medium such as thick tissue, however, the contribution of singly scattered photons is expected to be small and the majority of the detected photons will be multiply scattered. Further, unlike the ideal situation, in actual tissue, all the polarization effects are exhibited simultaneously and not in an ordered, sequential manner. To realize the potential of the Mueller matrix decomposition approach for quantification and interpretation of the useful polarization parameters (linear retardance and optical rotation in particular) in real tissues, it is necessary to test the validity of the decomposition process on multiply scattering media exhibiting simultaneous linear birefringence, optical activity, and depolarization. A quantitative understanding of the confounding effects of multiple scattering on the values for the polarization parameters estimated through the decomposition process is also essential.

We therefore investigate these aspects both theoretically and experimentally. The effects of multiple scattering, the propagation path of scattered photons, and detection geometry on the values for δ and ψ were studied systematically using polarization-sensitive Monte Carlo simulations of the propagation of polarized light in birefringent, chiral, multiply scattering media having varying optical properties. In the simulations, the simultaneous effects of linear birefringence and optical activity on the photons between successive scattering events were incorporated using the Jones N-matrix formalism.[32] In the corresponding experimental studies, Mueller matrices were recorded from realistic tissue phantoms exhibiting controllable scattering, linear birefringence, and optical activity. The values for the polarization parameters estimated through the decomposition process were compared with the known optical properties of the phantoms. The results of these theoretical investigations and the experimental studies are reported in this communication.

The organization of this paper is as follows. Section 2 provides a description of the experimental systems and methods as well as the optical phantoms used in this study. The forward polarization-sensitive Monte Carlo simulations of propagation of polarized light in multiply scattering media and the inverse process for polar decomposition of the resulting Mueller matrix are described in Sec. 3. The results of decomposition of the experimental and the Monte Carlo–generated Mueller matrices are presented in Sec. 4 to validate the method and to elucidate the observed trends. Section 5 concludes the paper with a discussion on the implications of these results and potential use of the Mueller matrix decomposition methodology in diagnostic photomedicine.

2 Experimental Methods and Materials

The Mueller matrices were recorded from the tissue phantoms using a photoelastic modulation (PEM)–based polarimeter.[7,32] A schematic of the experimental setup is shown in Fig. 1. Unpolarized light at 632.8 nm from a He-Ne laser (LHRR-1200M, Research Electro-Optics, Boulder, Colorado) was first passed through a mechanical chopper (C) operating at a frequency $f_c = 500$ Hz and then through a linear polarizer (P1)
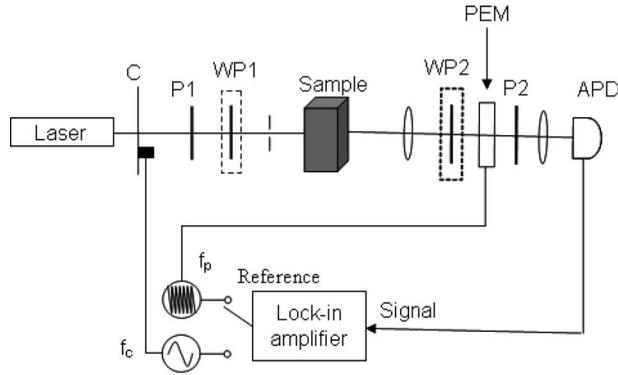
Fig. 1 Schematic of the experimental setup. C, mechanical chopper; P1 and P2, polarizers; WP1 and WP2, removable quarter wave plates, PEM, photoelastic modulator; APD, avalanche photodiode; f_c and f_p modulation frequencies of the chopper and PEM, respectively.

and a removable quarter wave plate (WP1). The linear polarizer and quarter wave plate combination enabled generation of the four required input polarization states, 0 deg (Stokes vector $[1\ 1\ 0\ 0]^T$), 45 deg (Stokes vector $[1\ 0\ 1\ 0]^T$), 90 deg (Stokes vector $[1\ -1\ 0\ 0]^T$) linear polarization, and circular polarization (Stokes vector $[1\ 0\ 0\ 1]^T$). The four set of Stokes vectors $[I\ Q\ U\ V]$ of light exiting the sample in selected detection directions were measured for each of the four input polarization states. For this study, we chose forward detection geometry; other detection geometries (including backscatter-

ing) are ongoing. The detection optics consists of another removable quarter wave plate (WP2) with its fast axis oriented at −45 deg. When WP2 was in place, we could measure the Stokes parameters Q and U (linear polarization),[7] and when it was removed, we could measure the Stokes parameter V (circular polarization).[32] The forward scattered light from the sample then passed through a photoelastic modulator (PEM, IS-90, Hinds Instruments, Hillsboro, Oregon, operating at a frequency $f_p = 50$ kHz) with its fast axis oriented at 0 deg. The light finally passed through an analyzer (P2) oriented at 45 deg. The resulting modulated intensity of the scattered light was collected using a pair of lenses (detection area of 1 mm^2 and acceptance angle $\sim$18 deg) and was relayed to an avalanche photodiode (APD) detector (C5460, Hamamatsu Photonics, Hamamatsu City, Japan). The detected signal was sent to a lock-in amplifier (SR 830, Stanford Research Systems, Sunnyvale, California) with reference input of the amplifier toggled between the chopper (500 Hz) and the PEM controller (50 kHz and harmonics).

The Stokes vector of the output light for each of the four input polarization states were measured using the detected signal at the first harmonic of the chopper frequency and the first and the second harmonics of the PEM frequencies.[7,32] The Mueller matrix was generated using standard relationships between its 16 elements and the measured output Stokes parameters $[I\ Q\ U\ V]$ for each of the four input polarization states.[28,29]

$$\begin{pmatrix} \begin{matrix} M(1,1) \\ 0.5 \times (I_H + I_V) \end{matrix} & \begin{matrix} M(1,2) \\ 0.5 \times (I_H - I_V) \end{matrix} & \begin{matrix} M(1,3) \\ [I_P - M(1,1)] \end{matrix} & \begin{matrix} M(1,4) \\ [I_R - M(1,1)] \end{matrix} \\ \begin{matrix} M(2,1) \\ 0.5 \times (Q_H + Q_V) \end{matrix} & \begin{matrix} M(2,2) \\ 0.5 \times (Q_H - Q_V) \end{matrix} & \begin{matrix} M(2,3) \\ [Q_P - M(2,1)] \end{matrix} & \begin{matrix} M(2,4) \\ [Q_R - M(2,1)] \end{matrix} \\ \begin{matrix} M(3,1) \\ 0.5 \times (U_H + U_V) \end{matrix} & \begin{matrix} M(3,2) \\ 0.5 \times (U_H - U_V) \end{matrix} & \begin{matrix} M(3,3) \\ [U_P - M(3,1)] \end{matrix} & \begin{matrix} M(3,4) \\ [U_R - M(3,1)] \end{matrix} \\ \begin{matrix} M(4,1) \\ 0.5 \times (V_H + V_V) \end{matrix} & \begin{matrix} M(4,2) \\ 0.5 \times (V_H - V_V) \end{matrix} & \begin{matrix} M(4,3) \\ [V_P - M(4,1)] \end{matrix} & \begin{matrix} M(4,4) \\ [V_R - M(4,1)] \end{matrix} \end{pmatrix}. \tag{1}$$

Here, the subscripts H, P, V, and R correspond to the measured Stokes parameters for state of polarization of incident light of 0-, 45-, and 90-deg linear polarization and circular polarization respectively. All the Mueller matrices were normalized with respect to the element $M(1,1)$.

The optical phantoms used in this study were polyacrylamide gels having strain-induced linear birefringence, sucrose-induced optical activity (magnitude of optical activity was $\chi = 1.96$ deg cm^{-1}, corresponding to 1 M concentration of sucrose) and polystyrene microspheres–induced scattering (mean diameter $D = 1.40$ μm, refractive index $n_s = 1.59$).[32,33] The refractive index of polyacrylamide was measured to be $n_m \sim 1.393$ at the wavelength $\lambda = 632.8$ nm. The phantom preparation details are described in Ref. 32. The values for

scattering coefficient (μ_s) of the phantoms at 632.8 nm were calculated using the known concentration of the scatterers and Mie theory.[34] The value for anisotropy parameter (g, average cosine of scattering angle) of the scattering phantom at 632.8 nm was calculated[34] to be $g = 0.95$.

To apply controllable strain to produce linear birefringence, one end of the polyacrylamide phantoms (dimension of $1 \times 1 \times 4$ cm) was clamped to a mount and the other end to a linear translational stage. The phantoms were stretched along the vertical direction (along the long axis of the sample) to introduce varying linear birefringence with its axis along the direction of strain. Mueller matrices were recorded in the forward detection geometry from the phantoms with varying extension (varying degree of strain-induced birefringence).

3 Theory

3.1 *Polarization-Sensitive Monte Carlo Simulations*

Polarization-sensitive Monte Carlo simulation software, developed in our group,[27,32,35] was used to generate the Mueller matrices of scattered light exiting the medium in the forward direction. In these simulations, the photons are propagated between scattering events, as determined by pseudorandom sampling of scattering mean free path, similar to conventional Monte Carlo model[36] for light propagation in a multiply scattering medium. The Mie theory[34] computed scattering phase function is used for sampling the scattering angles and computing the polarization changes of photons after successive scattering events. The polarization information is tracked in the form of a Stokes vector for each individual photon packet. The scattering histories of a large number of such photon packets are tracked as they propagate through the medium and are summed to yield the macroscopic polarization parameters of interest. To model the situation typically encountered in tissue, in addition to the multiple scattering effects, the simultaneous effects of linear birefringence and optical activity are also incorporated in the model. Note that this is not an obvious modeling step. Because matrix multiplication of the Mueller matrices are not commutative, different orders in which these effects are applied to the photon between scattering events will have different effects on the polarization. Therefore, this was accomplished by combining the effects into a single matrix describing them simultaneously, through the use of Jones N-matrix formalism[37,38] in the polarization-sensitive Monte Carlo simulation code. In this formalism, the matrix of the sample is represented as an exponential sum of differential matrices, known as N-matrices. Each matrix in this sum corresponds to a single optical property (e.g., linear birefringence or optical activity). These N-matrices are then used to express the M-matrix for the combined effect. The resulting M-matrix is applied to the photon between scattering events to model the simultaneous occurrence of linear birefringence and optical activity in a scattering medium. The details of this formalism are provided in Ref. 32.

Simulations were run for a given set of optical parameters of the scattering medium. The scattering phase function was computed using Mie theory for a set of input parameters, the diameter of scatterer (D), refractive index of scatterer (n_s), refractive index of the surrounding medium (n_m), and wavelength of light (λ). The computed phase function, the scattering coefficient (μ_s), and absorption coefficient (μ_a) of the medium were then used in the simulations. In the simulations, optical activity is specified as a rotation of χ in degrees per centimeter. Linear birefringence is modeled through the anisotropy in refractive indices (Δn), the difference in refractive index along the extraordinary axis (the axis along which the refractive index differs from other directions), and the ordinary axis. The anisotropy in refractive indices leads to a difference in the phase for light polarized parallel and perpendicular to the direction of the extraordinary axis. In this formalism, it is assumed that refractive index differs only along one axis (the extraordinary axis) and that the direction of the axis and the difference in refractive indices is constant throughout the scattering medium. In each simulation, a specific direction of this axis of linear birefringence was chosen. To generate the complete 16-element Mueller matrix, the state of polarization of incident light was changed sequentially to horizontal (Stokes vector $S_i=[1\ 1\ 0\ 0]^T$), vertical ($S_i=[1\ -1\ 0\ 0]^T$), +45 deg ($S_i=[1\ 0\ 1\ 0]^T$) linear polarization, and circular polarization ($S_i=[1\ 0\ 0\ 1]^T$); the Stokes vectors $[I\ Q\ U\ V]$ of light exiting the sample were recorded for each given incident polarization state. The Mueller matrix was generated using Eq. (1), the standard relationships between its 16 elements and the generated output Stokes parameters for the four input polarization states.[28,29]

The Mueller matrices were generated for a slab of scattering medium, having varying optical properties, for light exiting the medium in the forward direction. The average photon path length of light exiting the scattering medium was also recorded in the simulations. The photon collection geometry was chosen to have a detection area of 1 mm^2 and an acceptance angle of 20 deg to match the experiment. The absorption was selected to be small, and accordingly, the value for absorption coefficient (μ_a) was kept at 0.0001 mm^{-1} in all the simulations. To have satisfactory statistics, all the simulations were run with 1×10^8 input photons.

3.2 *Polar Decomposition of Mueller Matrices to Extract Individual Polarization Parameters*

Polar decomposition of Mueller matrix is a robust mathematical tool for interpretation of the polarization characteristics of any medium. The method decomposes an arbitrary Mueller matrix M into the product of three elementary matrices representing a depolarizer (M_Δ), a retarder (M_R), and a diattenuator (M_D). The process and its validity were first demonstrated by Lu and Chipman[30] in clear media. It is important to note that because the multiplication of the Mueller matrices is not commutative (as per the earlier N-matrix discussion), the results of the decomposition depend upon the order in which the three elementary matrices are multiplied. It has been shown previously that the six possible decompositions can be classified into two families, depending upon the order in which the depolarization and the diattenuator matrices are multiplied.[39] Because the family in which the diattenuator matrix comes ahead of the depolarizer matrix always lead to a physically realizable Mueller matrix,[39] this order of decomposition has been adopted in the present study.

$$M = M_\Delta M_R M_D. \tag{2}$$

3.2.1 *Diattenuation*

The diattenuation matrix M_D is defined as

$$M_D = \begin{bmatrix} 1 & \vec{d}^T \\ \vec{d} & m_D \end{bmatrix}. \tag{3}$$

Here m_D is a 3×3 submatrix (the standard form of which is provided in reference 30) $\vec{d}$ is the diattenuation vector and is defined as

$$\vec{d} = \{1/M(1,1)\} \times [M(1,2)\ M(1,3)\ M(1,4)]^T. \tag{4}$$

The magnitude of diattenuation can be determined as

$$d = \{1/M(1,1)\} \times [\{M(1,2)\}^2 + \{M(1,3)\}^2 + \{M(1,4)\}^2]^{1/2}. \tag{5}$$

Here $M(i,j)$ are elements of the Mueller matrix M. The coefficients $M(1,2)$ and $M(1,3)$ represent linear diattenuation for horizontal (vertical) and +45-deg (−45-deg) linear polarization, respectively, and the coefficient $M(1,4)$ represents circular diattenuation.

3.2.2 Depolarization

The decomposed depolarization matrix M_Δ has the form

$$M_\Delta = \begin{bmatrix} 1 & \vec{0}^T \\ \vec{P_\Delta} & m_\Delta \end{bmatrix}. \tag{6}$$

Here m_Δ is the 3×3 depolarization submatrix and the parameter P_Δ depends on polarizance (P) and diattenuation (d).[30]

The diagonal elements of the depolarization matrix M_Δ can be used to calculate the depolarization coefficients [$M_\Delta(2,2)$, $M_\Delta(3,3)$ are depolarization coefficients for incident horizontal (or vertical) and 45-deg linearly polarized light, and $M_\Delta(4,4)$ is the depolarization coefficient for incident circularly polarized light]. The net depolarization coefficient Δ is defined as

$$\Delta = 1 - \{|\mathrm{tr}(M_\Delta) - 1|/3\}. \tag{7}$$

Note that this definition of depolarization coefficient is different from the conventional Stokes parameter–based definition of degree of polarization [$= (Q^2 + U^2 + V^2)^{1/2}/I$]. The latter represents the value of degree of polarization resulting from several lumped polarization effects and also depends on the incident Stokes vector. In contrast, the depolarization coefficient (Δ) defined by Eq. (7) represents the pure depolarizing transfer function of the medium.

3.2.3 Retardance

The value for total retardance (R, a parameter that represents the combined effect of linear and circular birefringence) can be determined from the decomposed retardance matrix M_R using the relationship[30]

$$R = \cos^{-1}\left\{\frac{tr(M_R)}{2} - 1\right\}. \tag{8}$$

The total retardance matrix from the decomposition process can be further expressed as a combination of a matrix for a linear retarder (having a magnitude of linear retardance $= \delta$ and orientation angle of the axis of linear retarder with respect to the horizontal axis $= \theta$) and a circular retarder (optical rotation with magnitude of ψ)[31]

$$M_R = \begin{pmatrix} 1 & 0 & 0 & 0 \\ 0 & \cos^2 2\theta + \sin^2 2\theta \cos \delta & \sin 2\theta \cos 2\theta (1 - \cos \delta) & -\sin 2\theta \sin \delta \\ 0 & \sin 2\theta \cos 2\theta (1 - \cos \delta) & \sin^2 2\theta + \cos^2 2\theta \cos \delta & \cos 2\theta \sin \delta \\ 0 & \sin 2\theta \sin \delta & -\cos 2\theta \sin \delta & \cos \delta \end{pmatrix} \begin{pmatrix} 1 & 0 & 0 & 0 \\ 0 & \cos 2\psi & \sin 2\psi & 0 \\ 0 & -\sin 2\psi & \cos 2\psi & 0 \\ 0 & 0 & 0 & 1 \end{pmatrix}. \tag{9}$$

Using this standard form of the linear retardance and optical rotation matrices, the relationship between total retardance (R), optical rotation (ψ), and linear retardance (δ) can be worked out as

$$R = \cos^{-1}\left\{2 \cos^2(\psi)\cos^2\left(\frac{\delta}{2}\right) - 1\right\}. \tag{10}$$

The values for optical rotation (ψ) and linear retardance (δ) can be determined from the elements of the matrix M_R as

$$\psi = \tan^{-1}\{[M_R(3,2) - M_R(2,3)]/[M_R(2,2) + M_R(3,3)]\}, \tag{11}$$

$$\delta = \cos^{-1}(\{[M_R(2,2) + M_R(3,3)]^2 + [M_R(3,2) - M_R(2,3)]^2\}^{1/2} - 1). \tag{12}$$

It is important to note that although the multiplication of the linear retardance and optical rotation matrices are not commutative, the parameters R, ψ, and δ determined through Eqs.

(8), (11), and (12) are not influenced by the order of multiplication of the two matrices in Eq. (9).

Once the value for ψ is obtained, the optical rotation matrix formed using the value for ψ can be inverse multiplied with the total retardance matrix M_R to yield the linear retardance matrix (M_{LR}). The linear retardance matrix thus obtained can be written in the form

$$M_{LR} = \begin{pmatrix} 1 & \vec{0} \\ \vec{0} & m_{LR} \end{pmatrix}. \tag{13}$$

The elements of the linear retardance vector $\vec{LR} = [1, r_1, r_2, r_3]$ can be obtained using the elements of the 3×3 sub-matrix m_{LR} as[30]

$$r_i = (1/2 \sin \delta) \times \sum_{j,k=1}^{3} \varepsilon_{ijk} m_{LR}(j,k). \tag{14}$$

Here ε_{ijk} is Levi-Civita permutation symbol.

Table 1 (a) The experimentally recorded Mueller matrix and the decomposed basis matrices for a nonscattering phantom (μ_s=0 mm^{-1}) with strain-induced birefringence (extension of 4 mm) and a concentration of sucrose of 1 M (χ=1.96 deg cm^{-1}). (b) The values for the different polarization parameters extracted from the decomposed matrices.

$$M$$
$$\begin{pmatrix} 1.0000 & -0.0229 & 0.0027 & 0.0058 \\ -0.0186 & 0.9956 & -0.0361 & 0.0318 \\ -0.0129 & 0.0392 & 0.2207 & -0.9656 \\ 0.0014 & 0.0280 & 0.9706 & 0.2231 \end{pmatrix}$$

$$M_\Delta \qquad\qquad M_R \qquad\qquad M_D$$
$$\begin{pmatrix} 1.0000 & 0 & 0 & 0 \\ 0.0041 & 0.9969 & 0 & 0 \\ -0.0070 & 0 & 0.9915 & 0 \\ -0.0019 & 0 & 0 & 0.9966 \end{pmatrix} \begin{pmatrix} 1.0000 & 0 & 0 & 0 \\ 0 & 0.9988 & -0.0362 & 0.0281 \\ 0 & 0.0393 & 0.2227 & -0.9741 \\ 0 & 0.0320 & 0.9742 & 0.2239 \end{pmatrix} \begin{pmatrix} 1.0000 & -0.0229 & 0.0027 & 0.0058 \\ -0.0229 & 1.0000 & -0.0000 & -0.0001 \\ 0.0027 & -0.0000 & 0.9997 & 0.0000 \\ 0.0058 & -0.0001 & 0.0000 & 0.9997 \end{pmatrix}$$

Parameters	Estimated Values
R	1.346 (rad)
d	0.024
δ, θ	1.345 (rad), 89.05 deg
ψ	1.77 deg
Δ	0.995

This then allows us to determine the orientation angle θ of the axis of linear retardance (with respect to the horizontal axis) from the elements of the retardance vector as

$$\theta = 0.5 \tan^{-1}(r_2/r_1). \tag{15}$$

The decomposition process just described was applied to the experimental Mueller matrices recorded from the poly-acrylamide phantoms and to the Mueller matrices generated through Monte Carlo simulations. The values for diattenuation (d), depolarization coefficient (Δ), total retardance (R), optical rotation (ψ), and linear retardance (δ and its orientation angle θ) were determined from the decomposed matrices using Eqs. (5), (7), (8), (11), (12), and (15), respectively. It should be mentioned that decomposition of a Mueller matrix from a multiply scattering medium exhibiting simultaneous linear birefringence and optical activity results in small but nonzero values for the off-diagonal elements of the depolarization submatrix m_Δ [following Eq. (6)]. In an ideal situation, m_Δ should be a diagonal matrix with zero off-diagonal elements and its three diagonal elements represent depolarization coefficients for 0- and 45-deg linear polarizations and circular polarization. The nonzero values for the off-diagonal elements of the decomposed depolarization submatrix m_Δ arise because unlike the ordered multiplication of the three elementary matrices of a depolarizer, a retarder, and a diattenuator, in a birefringent chiral turbid medium, the individual constituent polarization effects are exhibited in an arbitrary order. To facilitate quantitative comparison of the depolarization strength of incident linearly [depolarization coefficients $M_\Delta(2,2)$ and $M_\Delta(3,3)$] and circularly [depolarization coeffi-

cient $M_\Delta(4,4)$] polarized light, the depolarization submatrix m_Δ was presented in a diagonalized form for all the Mueller matrix decompositions. This way of representing the depolarizer matrix did not influence the polarization parameters estimated through the decomposition process.

4 Results and Discussion

Mueller matrices were experimentally recorded in the forward scattering geometry from the polyacrylamide phantoms having varying degrees of strain-induced birefringence (extension=0 to 4 mm applied along the vertical direction), varying scattering coefficients (μ_s=0, 3, 4, and 6 mm^{-1}), and sucrose-induced optical activity (concentration of 1 M corresponding to magnitude of optical activity χ=1.96 deg cm^{-1}). Measurements were also performed on a clear (nonscattering) polyacrylamide phantom at different extensions to obtain the calibration curve for the strain-induced birefringence with extension. Measurements were performed three times from each of the experimental phantoms and the mean values were taken to construct the Mueller matrices. Standard deviations in the values for the normalized Mueller matrix elements were found to be in the range 0.0015 to 0.0050.

Table 1 shows the experimental Mueller matrix and the decomposed (following the procedure described in Sec. 3.2) depolarization (M_Δ), retardance (M_R), and diattenuation (M_D) matrices for the nonscattering phantom (μ_s=0 mm^{-1}, thickness t=10 mm) with extension of 4 mm and having a concentration of sucrose of 1 M. The values for all the retrieved polarization parameters [R, d (δ and θ), ψ, and Δ, determined from the equations in Secs. 3.2.1, 3.2.2, and 3.2.3]

Table 2 (a) The experimentally recorded Mueller matrix and the decomposed basis matrices for a nonbirefringent (extension=0 mm), achiral (concentration of sucrose=0 M, $\chi=$ deg cm^{-1}), turbid phantom (optical thickness $\tau=30$, $\mu_s=3$ mm^{-1}, thickness $t=10$ mm, $g=0.95$). (b) The values for the different polarization parameters extracted from the decomposed matrices.

$$M$$
$$\begin{pmatrix} 1.0000 & -0.0190 & 0.0030 & 0.0114 \\ -0.0183 & 0.7454 & -0.0025 & 0.0019 \\ 0.0013 & 0.0085 & 0.7378 & -0.0648 \\ 0.0034 & 0.0037 & 0.0747 & 0.8530 \end{pmatrix}$$

$$M_\Delta$$
$$\begin{pmatrix} 1.0000 & 0 & 0 & 0 \\ -0.0042 & 0.7468 & 0 & 0 \\ 0.0000 & 0 & 0.7394 & 0 \\ -0.0065 & 0 & 0 & 0.8566 \end{pmatrix}$$

$$M_R$$
$$\begin{pmatrix} 1.0000 & 0 & 0 & 0 \\ 0 & 1.0000 & -0.0076 & -0.0005 \\ 0 & 0.0075 & 0.9961 & -0.0874 \\ 0 & 0.0012 & 0.0874 & 0.9962 \end{pmatrix}$$

$$M_D$$
$$\begin{pmatrix} 1.0000 & -0.0190 & 0.0030 & 0.0114 \\ -0.0190 & 0.9999 & -0.0000 & -0.0001 \\ 0.0030 & -0.0000 & 0.9998 & 0.0000 \\ 0.0114 & -0.0001 & 0.0000 & 0.9998 \end{pmatrix}$$

Parameters	Estimated Values
R	0.088 (rad)
d	0.022
δ	0.087 (rad)
ψ	0.22 deg
Δ	0.781

are also listed in the table. As expected, the nonscattering phantom does not show any appreciable depolarization ($\Delta \sim 1$). The value for δ is ~ 1.345 rad for an extension of 4 mm and the estimated orientation angle of the axis of linear retardance ($\theta=89.05$ deg) is reasonably close to the actual orientation of the linear birefringence axis ($\theta=90$ deg for strain applied along the vertical direction). The value for δ increased from 0.088 to 1.345 rad for varying extension of 0 to 4 mm. Due to presence of optical rotation, the estimated value for the total retardance parameter R [that represents the combined effect of linear retardance and optical rotation, see Eq. (10)] is marginally larger ($R=1.346$ rad) than the corresponding value for δ. The estimate for ψ (1.77 deg), however, is, lower than that expected for concentration of sucrose of 1 M ($\psi=1.96$ deg for a path length of 10 mm). The contraction of the phantom due to longitudinal stretching reduces the effective path length of transmitted light, contributing to the observed lower value of ψ. The reduction in path length at 4-mm extension is ~ 0.33 mm (path length of 9.67 mm as compared with 10 mm for the phantom with no strain) using the value for Poisson ratio (~ 0.33) of polyacrylamide.[32,40] However, even when accounting for this thickness reduction, the new expected ψ (1.90 deg) is still higher than the one derived from polar decomposition. This difference is possibly due to an uncertainty in the concentration of sucrose during the fabrication of the phantom. It is also seen from Table 1 that decomposition of Mueller matrix yields a small but nonzero value for the diattenuation parameter d. The presence of a small amount of dichroic absorption (at $\lambda=632.8$ nm) due to anisotropic alignment of the polymer molecules in the

polyacrylamide phantom may contribute to this slight nonzero value of diattenuation.

Table 2 displays the experimental Mueller matrix, the decomposed basis matrices, and the retrieved polarization parameters for a nonbirefringent (extension=0 mm), achiral (concentration of sucrose=0 M, $\chi=0$ deg cm^{-1}), turbid phantom ($\mu_s=3$ mm^{-1}, $t=10$ mm, optical thickness $\tau=\mu_s \times t=30$, $g=0.95$). Ideally, the Mueller matrix of this phantom should model an isotropic depolarizer. The values for δ, d, and ψ obtained following decomposition are indeed found to be low for this nonbirefringent, achiral sample. The small nonzero value for δ (0.087) may arise due to the small amount of strain present during clamping of the sample to the mount and translational stage. Another possible cause, the scattering-induced linear retardance,[31] which arises primarily from singly (or weakly) scattered photons, is not expected to contribute to the nonzero value for δ, because for this scattering sample having a value for optical thickness $\tau=30$, multiply scattered photons are the dominant contributor to the detected photons in the forward detection geometry. Further, in agreement with previous reports,[23–25] for this anisotropic scattering sample ($g=0.95$, prepared using large-sized scatterer with diameter $D \geq \lambda$), depolarization of circularly polarized light is weaker than depolarization of linearly polarized light [$M_\Delta(4,4) > M_\Delta(2,2)$ and $M_\Delta(3,3)$]. This was previously shown to arise due to the fact that in scattering media composed of large scatterers $D \geq \lambda, g \geq 0.7$, the randomization of helicity (which is the major cause of depolarization of circularly polarized light) is considerably reduced due to predominantly forward scattering, leading to weaker depolarization of

Table 3 (a) The experimentally recorded Mueller matrix and the decomposed basis matrices for a birefringent (extension=4 mm), chiral (concentration of sucrose=1 M, χ=1.96 deg cm^{-1}), turbid (μ_s=3 mm^{-1}, g=0.95) phantom. (b) The values for the different polarization parameters extracted from the decomposed matrices.

$$M$$

$$\begin{pmatrix} 1.0000 & -0.0312 & 0.0029 & -0.0066 \\ -0.0214 & 0.7678 & -0.0370 & 0.0204 \\ -0.0055 & 0.0230 & 0.1043 & -0.7735 \\ 0.0014 & 0.0390 & 0.7972 & 0.1920 \end{pmatrix}$$

$$M_\Delta \qquad\qquad\qquad M_R \qquad\qquad\qquad M_D$$

$$\begin{pmatrix} 1.0000 & 0 & 0 & 0 \\ 0.0028 & 0.7552 & 0 & 0 \\ -0.0102 & 0 & 0.7689 & 0 \\ 0.0016 & 0 & 0 & 0.8454 \end{pmatrix} \begin{pmatrix} 1.0000 & 0 & 0 & 0 \\ 0 & 0.9984 & -0.0513 & 0.0242 \\ 0 & 0.0333 & 0.1844 & -0.9823 \\ 0 & 0.0460 & 0.9815 & 0.1858 \end{pmatrix} \begin{pmatrix} 1.0000 & -0.0312 & 0.0029 & -0.0066 \\ -0.0312 & 1.0000 & -0.0000 & 0.0001 \\ 0.0029 & -0.0000 & 0.9995 & -0.0000 \\ -0.0066 & 0.0001 & -0.0000 & 0.9995 \end{pmatrix}$$

Parameters	Estimated Values
R	1.385 (rad)
d	0.032
δ, θ	1.384 (rad), 88.72 deg
ψ	2.04 deg
Δ	0.790

circularly polarized light.[23–25] Note that the depolarization of linearly polarized light is almost independent of the orientation angle (horizontal, vertical, and 45 deg) of the incident linear polarization vector [depolarization coefficients $M_\Delta(2,2) \sim M_\Delta(3,3)$]. This makes sense because in an isotropic, multiply scattering medium, randomization of the field vector's direction is the primary cause of depolarization of incident linearly polarized light. The linear depolarization coefficients of the resultant depolarizing Mueller matrix in such a situation will be the same for any orientation of the incident linear polarization vector.[41]

The experimental Mueller matrix, the decomposed basis matrices, and the retrieved polarization parameters for the birefringent (extension=4 mm), chiral (1 M sucrose, χ =1.96 deg cm^{-1}), and turbid phantom (μ_s=3 mm^{-1}, g=0.95) are shown in Table 3. Note the complicated nature of the Mueller matrix of this complex phantom and relatively unequivocal nature of the three basis matrices derived from the decomposition process. The elements of the depolarization matrix (M_Δ) and the resulting value for the depolarization coefficient (Δ) are similar to the corresponding values for the pure depolarizing phantom having the same scattering coefficient μ_s (Table 2, difference in the value for $\Delta < 2\%$). The decomposition process thus successfully decouples the depolarization effects (due to multiple scattering) and retrieves the values for the parameters δ (and θ) and ψ. However, the estimate for ψ is found to be larger than that for the clear phantom having the same concentration of sucrose (ψ=2.04 deg for the scattering phantom as compared with 1.77 deg for the clear phantom). This is due to the increase in the propagation

path of light in a multiply scattering medium. The average photon path length of light exiting the scattering sample in the forward direction was calculated to be 11.7 mm from Monte Carlo simulation (optical parameters of the medium: μ_s =3 mm^{-1}, diameter of scatterer D=1.40 μm, n_s=1.59, n_m =1.393, g=0.95). For the calculation of average photon path length, the thickness of the scattering medium was taken to be 9.67 mm as per the Poisson ratio discussion earlier. The value for ψ calculated using the optical rotation of the nonscattering phantom (ψ=1.77 deg from Table 1) and the Monte Carlo–generated average photon path length comes out to be reasonably close to that estimated through decomposition of the Mueller matrix recorded from the birefringent, chiral, turbid phantom (calculated value of ψ=2.07 deg as compared with ψ=2.04 deg estimated for the turbid phantom).

Although the estimated value for δ of the turbid phantom is larger than that for the clear phantom (δ=1.384 rad for the turbid phantom as compared with 1.345 rad for the clear phantom having a path length of 10 mm), the value is lower than that one would expect for average photon path length of 11.7 mm (δ=1.345$\times$1.17=1.574 rad). This is illustrated in Fig. 2 where the estimates for δ and ψ of the chiral (χ =1.96 deg cm^{-1}) phantoms having varying degrees of strain-induced birefringence (extension of 0 to 4 mm) are displayed. Results are shown for both the clear (μ_s=0 mm^{-1}) and the turbid (μ_s=3 mm^{-1}) phantoms. The increase in the value for ψ as a result of increased average photon path length in the turbid phantom as compared with the clear phantom can be seen quite clearly. The gradual decrease in the value for ψ

Fig. 2 The values for linear retardance (δ) and optical rotation (ψ) estimated from the decomposition of experimentally recorded Mueller matrices from the chiral ($\chi=1.96$ deg cm^{-1}) phantoms having varying degrees of strain-induced birefringence (extension of 0 to 4 mm). Results are shown for both clear ($\mu_s=0$ mm^{-1}) and turbid ($\mu_s=3$ mm^{-1}) phantoms.

with increasing longitudinal stretching is consistent with resulting lateral contraction of the phantom, reducing the effective path length. In contrast to ψ, the expected increase in δ as a result of increased average photon path length in the turbid phantom is not seen. The results of studies on phantoms hav-

ing other values of scattering coefficients ($\mu_s=4$ and 6 mm^{-1}, data not shown) also yielded similar trends to that observed for the phantom with $\mu_s=3$ mm^{-1}.

To understand these trends further and to investigate the effect of multiple scattering, propagation path, and detection geometry on δ and ψ parameters, Monte Carlo simulations were carried out.

The Monte Carlo simulations were run with input optical parameters chosen to mimic the optical properties of the phantoms used in the experimental studies. The photon collection geometry was chosen to have a detection area of 1 mm^2 and an acceptance angle of 20 deg around the forward directed ballistic beam. Standard deviations (originating from random statistical errors) in the different elements of the Monte Carlo–generated Mueller matrices were found to be in the range 0.0004 to 0.0025. Table 4 shows the Mueller matrix, the decomposed basis matrices, and the retrieved polarization parameters for a nonbirefringent, achiral, turbid medium (linear birefringence $\Delta n=0$, $\chi=0°$ cm^{-1}, $\tau=30$, $\mu_s=3$ mm^{-1}, $t=10$ mm) composed of monodisperse spherical scatterers ($D=1.40$ μm, $n_s=1.59$, $n_m=1.393$, $g=0.95$). In agreement with the experimental results (Table 2), polarization preservation of circularly polarized light is found to be larger than linearly polarized light [$M_\Delta(4,4)>M_\Delta(2,2)$ and $M_\Delta(3,3)$] for this forward scattering ($g=0.95$) turbid medium. The elements of the decomposed depolarization matrix M_Δ are also close to the experimental Mueller matrix results (difference in the value for $\Delta \sim 4\%$) for the phantom having similar scattering coefficient (small differences may arise due to slight mis-

Table 4 (a) The Monte Carlo simulation–generated Mueller matrix and the decomposed basis matrices for a nonbirefringent, achiral, turbid medium ($\Delta n=0$, $\chi=0$ deg cm^{-1}, $\tau=30$, $\mu_s=3$ mm^{-1}, $t=10$ mm, $g=0.95$). (b) The values for the different polarization parameters extracted from the decomposed matrices.

$$
M
$$
$$
\begin{pmatrix}
1.0000 & -0.0025 & -0.0026 & -0.0024 \\
-0.0008 & 0.7787 & 0.0001 & 0.0009 \\
-0.0020 & 0.0003 & 0.7767 & 0.0034 \\
0.0002 & 0.0004 & -0.0004 & 0.8809
\end{pmatrix}
$$

$$
M_\Delta \qquad\qquad M_R \qquad\qquad M_D
$$
$$
\begin{pmatrix}
1.0000 & 0 & 0 & 0 \\
0.0012 & 0.7788 & 0 & 0 \\
0.0000 & 0 & 0.7766 & 0 \\
0.0024 & 0 & 0 & 0.8810
\end{pmatrix}
\begin{pmatrix}
1.0000 & 0 & 0 & 0 \\
0 & 1.0000 & -0.0001 & 0.0003 \\
0 & 0.0001 & 1.0000 & 0.0023 \\
0 & -0.0003 & -0.0023 & 1.0000
\end{pmatrix}
\begin{pmatrix}
1.0000 & -0.0025 & -0.0026 & -0.0024 \\
-0.0025 & 1.0000 & 0.0000 & 0.0000 \\
-0.0026 & 0.0000 & 1.0000 & 0.0000 \\
-0.0024 & 0.0000 & 0.0000 & 1.0000
\end{pmatrix}
$$

Parameters	Estimated Values
R	0.0023 (rad)
d	0.004
δ	0.0023 (rad)
ψ	0.003 deg
Δ	0.812

Fig. 3 Variation of the parameters δ, d, ψ, and Δ (estimated from the decomposition of Monte Carlo–generated Mueller matrices) as a function of optical thickness τ (varying μ_s and fixed thickness of t =10 mm) for nonbirefringent ($\Delta n=0$), achiral ($\chi=0$ deg cm^{-1}), turbid medium composed of monodisperse spherical scatterers (D =1.40 μm, n_s=1.59, n_m=1.393, g=0.95). The results are shown for transmitted light collected from the ballistic beam position at the exit face of the medium.

match in the collection geometry employed in the experiments and in the simulation, and possibly due to subtle errors in concentration of scatterers in the phantom). Further, as expected, the values for δ, d, and ψ of this nonbirefringent, achiral, turbid medium are also small. The small value of δ

(0.0023 rad) for this nonbirefringent turbid medium confirms that scattering-induced linear retardance should not contribute to the experimentally observed slightly larger value for δ (0.087 rad) for the phantom having the same scattering coefficient of μ_s=6 mm^{-1}.

Figure 3 shows the variation of the parameters d, δ, Δ, and ψ of transmitted light as a function of optical thickness τ (varying μ_s and fixed path length of t=10 mm) for the non-birefringent, achiral, turbid medium. As expected, depolarization decreases with increasing value of τ. In the absence of chiral molecules, the values for ψ are low at all the optical thickness values of the achiral, turbid medium. Further, both the parameters δ and d are <0.02 for the range of τ=10 to 80. As discussed previously, the scattering-induced linear retardance and diattenuation arises primarily from singly (or weakly) scattered photons and the magnitude is greater at large scattering angles. Because for detection around the forward direction, the contribution of such photons is negligible, the scattering-induced retardance and diattenuation are weak in this geometry.

Table 5 presents the Monte Carlo–generated Mueller matrix, the decomposed basis matrices, and the retrieved polarization parameters for a birefringent, chiral, turbid medium ($\Delta n=1.36\times10^{-5}$, corresponding to δ=1.35 rad for a path length of t=10 mm, optical activity χ=1.96 deg cm^{-1}, τ =30, μ_s=3 mm^{-1}, g=0.95). The axis of linear birefringence was along the vertical (y, θ=90 deg) direction in the simulation. The values for δ and ψ estimated following the decomposition process are reasonably close to those of the experimental phantom having similar properties (Table 3). Slightly

Table 5 (a) The Monte Carlo simulation–generated Mueller matrix and the decomposed basis matrices for a birefringent, chiral, turbid medium ($\Delta n=1.36\times10^{-5}$, χ=1.96 deg cm^{-1}, τ=30, μ_s=3 mm^{-1}, t=10 mm, g=0.95). (b) The values for the different polarization parameters extracted from the decomposed matrices.

$$M$$
$$\begin{pmatrix} 1.0000 & -0.0039 & 0.0022 & -0.0097 \\ 0.0012 & 0.7742 & 0.0310 & -0.0393 \\ -0.0061 & -0.0429 & 0.1234 & -0.7949 \\ -0.0009 & -0.0251 & 0.8146 & 0.1983 \end{pmatrix}$$

$$M_\Delta \qquad\qquad M_R \qquad\qquad M_D$$
$$\begin{pmatrix} 1.0000 & 0 & 0 & 0 \\ 0.0038 & 0.7758 & 0 & 0 \\ -0.0142 & 0 & 0.7836 & 0 \\ -0.0009 & 0 & 0 & 0.8595 \end{pmatrix} \begin{pmatrix} 1.0000 & 0 & 0 & 0 \\ 0 & 0.9979 & 0.0412 & -0.0490 \\ 0 & -0.0561 & 0.1948 & -0.9792 \\ 0 & -0.0308 & 0.9800 & 0.1967 \end{pmatrix} \begin{pmatrix} 1.0000 & -0.0039 & 0.0022 & -0.0097 \\ -0.0039 & 1.0000 & -0.0000 & 0.0000 \\ 0.0022 & -0.0000 & 0.9999 & -0.0000 \\ -0.0097 & 0.0000 & -0.0000 & 1.0000 \end{pmatrix}$$

Parameters	Estimated Values
R	1.375 (rad)
d	0.011
δ, θ	1.373 (rad), 88.57 deg
ψ	2.33 deg
Δ	0.8063

larger disagreement in ψ ($\sim 14\%$) possibly arises due to an uncertainty in the concentration of sucrose during the fabrication of the phantom (as noted previously). Incorporation of the path length reduction due to longitudinal stretching ($t = 9.67$ mm as compared with $t = 10$ mm) in the simulations did not result in significant changes in the estimated values for δ and ψ (reduction in δ and ψ were $\leqslant 3\%$). As for the nonbirefringent, achiral, turbid medium (Table 4), this birefringent, chiral, turbid medium prepared using large-sized scatterers (diameter $D \geqslant \lambda$) also exhibits weaker depolarization of circularly polarized light than linearly polarized light $[M_\Delta(4,4) > M_\Delta(2,2), M_\Delta(3,3)]$. The elements of M_Δ and the resulting value for Δ are also similar to the corresponding values for the nonbirefringent, achiral, turbid medium with the same scattering properties.

Note that at an even larger value of the input linear birefringence ($\Delta n > 1.36 \times 10^{-5}$), the decomposed circular depolarization coefficient $[M_\Delta(4,4)]$ was found to be lower than the corresponding value for the nonbirefringent, turbid medium (the trend can be seen from Tables 4 and 5 also). Because for this forward scattering medium ($g \sim 0.95$), depolarization of circularly polarized light is weaker than depolarization of linearly polarized light,[23–25] while propagating through such a birefringent (with axis of birefringence along the vertical direction), turbid medium, a greater fraction of incident circularly polarized light gets transferred to 45-deg linear polarization as compared with transfer of 45-deg linear polarization to circular polarization. This also led to a difference in the value for the depolarization coefficient for 45-deg linearly polarized light and horizontally (or vertically) polarized light $[M_\Delta(3,3) \neq M_\Delta(2,2)]$. This suggests that even in the presence of strong multiple scattering, for a turbid medium that exhibits linear birefringence, the depolarization of linearly polarized light may depend on the orientation angle of the incident linear polarization vector.

To gain quantitative understanding of the dependence of the δ and ψ parameters on the propagation path of multiply scattered photons, Fig. 4 shows the Monte Carlo results for the variation of δ and ψ as a function of the thickness of the same birefringent, chiral, scattering medium. The top axis shows the calculated average photon path length of light exiting the scattering medium. The value for ψ increases with increasing average photon path length. However, the absolute values for ψ were marginally lower compared to calculations using the linear relationship ($\psi = \chi \times$ average photon path length). It should be noted here that the average path length has contributions from both the polarization-preserving and the depolarized photons. The fact that the propagation path of the polarization-preserving photons (which would show experimentally detectable optical rotation) is shorter than the average photon path length[42] should account for the observed lower value for ψ.

It is interesting that although the value for δ increases with increasing average photon path length, the increase is much slower as compared with ψ. A similar trend was also observed in the experimental studies. This is because in a turbid medium, the forward scattered light does not travel in a straight line but rather along a curved path, the curvature being controlled by the values for μ_s and g. Though such paths do not have any influence on ψ (as long as the average photon path
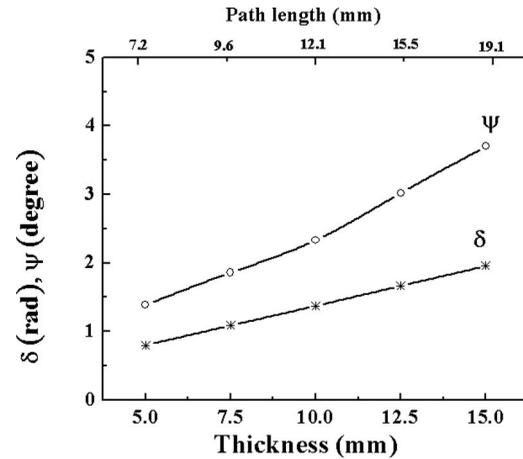
Fig. 4 Variation of δ and ψ (estimated from the decomposition of Monte Carlo–generated Mueller matrices) as a function of the thickness of a birefringent ($\Delta n = 1.36 \times 10^{-5}$, corresponding to a value of $\delta = 1.35$ for path length of 10 mm), chiral ($\chi = 1.96$ deg cm^{-1}), turbid medium ($\mu_s = 3$ mm^{-1}, $\tau = 30$, $g = 0.95$). The Monte Carlo–calculated average photon path length of light exiting the scattering medium is shown on the top axis.

length is the same), the net value for δ would be significantly affected because the linear birefringence has a specific orientation axis ($\theta = 90$ deg in the simulations and in the experiments).

To understand this, Mueller matrices were generated for transmitted light collected at the exit face of the birefringent ($\Delta n = 1.36 \times 10^{-5}$ and 0.68×10^{-5}), chiral ($\chi = 1.96$ deg cm^{-1}), turbid medium ($\tau = 30$, $\mu_s = 3$ mm^{-1}, $g = 0.95$) at different spatial positions away from the position of the ballistic beam along the horizontal (x axis, perpendicular to the direction of linear birefringence) and vertical (y axis, parallel to the direction of linear birefringence) directions. The variations for the parameter δ as a function of the distance from the ballistic beam position (along both x and y axis) at the exit face are displayed in Fig. 5. At spatial positions along the x axis, δ increases with increasing distance from the center of the ballistic beam (i.e., with increasing average photon path length). In contrast, for detection at spatial positions along the y axis, the value for δ shows gradual decrease with increasing distance from the center of the ballistic beam. This is because a larger component of the photon propagation path is along the axis of birefringence leading to a reduction in net linear retardance δ (because propagation along the direction of the birefringence axis does not yield any retardance). Because such differences in the photon propagation path for the two different detection geometries should have no influence on ψ, the estimates for ψ were found to be identical for similar detection positions either along the x or the y axis at the exit face of the medium (data not shown). It thus appears that the value for δ is influenced by the detection position and the orientation angle of the axis of linear birefringence in a birefringent, turbid medium.

To examine this further, in Fig. 6, we show the variation of δ as a function of the orientation angle (θ) of the axis of linear birefringence for the birefringent, chiral, turbid medium ($\Delta n = 1.36 \times 10^{-5}$, $\chi = 1.96$ deg cm^{-1}, $\tau = 30$, $\mu_s = 3$ mm^{-1}, g
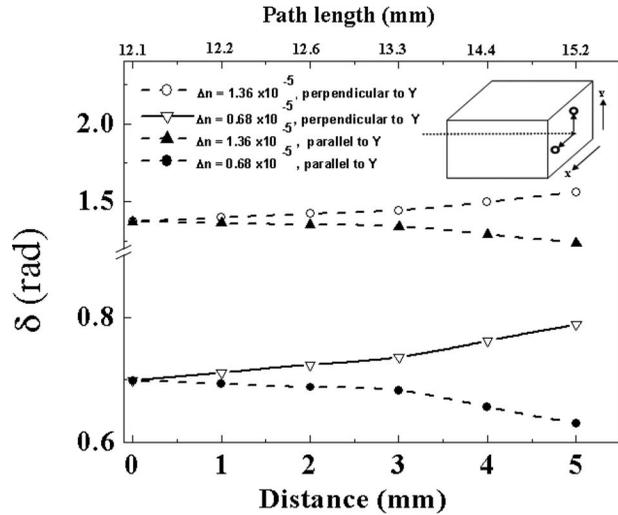
Fig. 5 Variation of δ (estimated from the decomposition of Monte Carlo–generated Mueller matrices) of transmitted light as a function of distance from ballistic beam position at the exit face of a birefringent, chiral ($\chi = 1.96$ deg cm^{-1}), turbid medium ($\tau = 30$, $\mu_s = 3$ mm^{-1}, $g = 0.95$). The results are shown for two different values of birefringence ($\Delta n = 1.36 \times 10^{-5}$ and 0.68×10^{-5}). The axis of linear birefringence was kept along the vertical (y axis) direction and the results are shown for transmitted light collected at different spatial positions along the horizontal (x axis, perpendicular to the direction of the axis of birefringence) and vertical (y axis, parallel to the direction of the axis of birefringence) direction at the exit face of the medium. The Monte Carlo–calculated average photon path length of light exiting the scattering medium is shown on the top axis. The inset shows the detection geometry.

$= 0.95$). Results are shown for three different detection positions at the exit face of the medium, around the position of the ballistic beam [coordinate (0,0)], at 3 mm away from the position of the ballistic beam along the horizontal (x) [coordi-
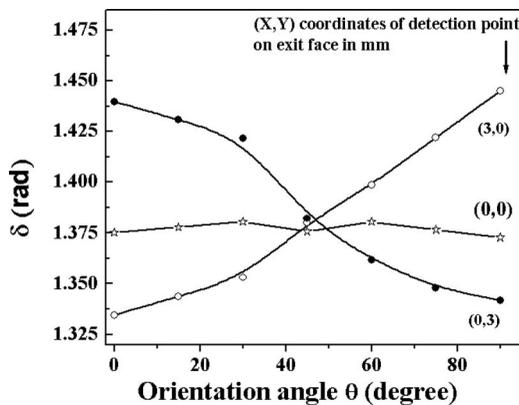
Fig. 6 Variation of δ (estimated from the decomposition of Monte Carlo–generated Mueller matrices) as a function of the orientation angle θ (with respect to the horizontal axis) of the axis of linear birefringence for a birefringent, chiral, turbid medium ($\Delta n = 1.36 \times 10^{-5}$, $\chi = 1.96$ deg cm^{-1}, $\tau = 30$, $\mu_s = 3$ mm^{-1}, $g = 0.95$). Results are shown for three different detection positions at the exit face of the medium, detection around the position of the ballistic beam [position coordinate (0,0)], detection at spatial positions 3 mm away from the ballistic beam position along the horizontal (x) [coordinate (3,0)] and vertical (y) [position coordinate (0,3)] axis, respectively.

nate (3,0)] and vertical (y) [coordinate (0,3)] axes, respectively. The value for δ is observed to vary considerably with a change in the birefringence orientation angle for off-axis detection [at spatial positions (3,0) or (0,3)]. As noted previously, the minimum values for δ are found at spatial positions along the direction of the birefringence axis. Due to the symmetry of position coordinates with respect to the direction of birefringence axis, the two values of δ [for spatial positions (3,0) and (0,3)] are also observed to converge for the value of $\theta = 45$ deg. In contrast, for detection around the position of the ballistic beam [coordinate (0, 0)], the estimates for δ do not show any significant variation with a change in the orientation angle of the axis of birefringence. Thus for simultaneous determination of the intrinsic values for the parameters δ and ψ of a birefringent, chiral, turbid medium in the forward scattering geometry, detection around the direction of propagation of the ballistic beam may be preferable.

The presented results demonstrate that decomposition of the Mueller matrix can be used for simultaneous determination of the intrinsic parameters δ (and θ) and ψ of a birefringent, chiral, turbid medium. For conceptual and practical reasons, the extension of the developed methodology to backward detection geometry is warranted. However, this will be more complex, because in the backward detection geometry, the contribution of backscattered (large angle scattered) photons would be greater and thus the interplay of the scattering-induced linear retardance and diattenuation with the intrinsic values for δ and ψ would be more coupled. Future studies will investigate this aspect in detail and will concentrate on developing an appropriate strategy to minimize the scattering-induced artifacts for simultaneous determination of δ and ψ in the backscattering geometry using Mueller matrix decomposition.

5 Conclusions

We have investigated the validity of Mueller matrix decomposition methodology to extract the individual intrinsic polarimetry characteristics from a multiply scattering medium exhibiting simultaneous linear birefringence and optical activity. Decomposition of experimental Mueller matrices recorded from tissue phantoms exhibiting controllable scattering, linear birefringence, and optical activity yielded satisfactory estimates for linear retardance δ and optical rotation ψ. Reliable estimates for linear and circular depolarization coefficients were also obtained. The effects of multiple scattering, the propagation path of scattered photons, and detection geometry on δ and ψ were further investigated using polarization-sensitive Monte Carlo simulations. The simulation results were found to corroborate the experimental findings and demonstrate that the Mueller matrix decomposition methodology can successfully extract the individual polarization characteristics of a medium that exhibits simultaneous linear birefringence, optical activity, and multiple scattering effects.

The ability of this technique to determine the constituent contributions of individual processes should prove valuable in diagnostic photomedicine. The value for linear retardance estimated using this approach would represent its average value over the volume of the turbid medium (tissue) probed by the polarization-preserving photons[43] and could monitor changes in tissue birefringence as a signature of tissue abnormality

and/or response to therapy. Note that in actual tissues due to larger value of μ_s and due to presence of absorption, the sampling depth of the polarization-preserving photons will be considerably reduced (typically a few millimeters) as compared with that of the phantoms used in this study. As a representative application, we are currently investigating the use of the decomposition-derived linear retardance for monitoring myocardial tissue regeneration following stem cell treatments of myocardial infarction. Measurement (in the forward detection geometry) through $\sim$1-mm thick *ex vivo* myocardial tissue samples are yielding encouraging results and show promise for the use of this approach for monitoring of stem-cell–based treatments of myocardial infarction. These results will be reported in a separate publication. Further, the decomposition method may also find useful applications in quantifying the optical rotations due to blood glucose in diabetic patients, potentially impacting the (currently unsolved) noninvasive glucose-monitoring problem. The results presented here demonstrate the ability to quantify optical activity (albeit at higher than physiological levels) despite depolarization and other effects in multiply scattering media, using the decomposition methodology. Ordinarily, the small chirality-caused optical rotation is swamped by much larger scattering-induced rotation, and it is the decomposition method that enables the glucose-related signal to be derived and quantified from the Mueller matrix results. The application of this approach to real tissues with lower blood glucose levels ($\sim$3 to 30 mM), however, will require further refinements of the highly sensitive Mueller matrix measurements to detect small changes in the matrix elements corresponding to the physiological glucose levels. This and the combined use of the Mueller matrix decomposition approach and spectroscopic polarimetry (coupled with chemometric data analysis to isolate the rotation due to glucose from that caused by other chiral constituent confounders in tissue) is currently under investigation in our laboratory.

Acknowledgments

References

1. L. V. Wang, G. L. Côté, and S. L. Jacques, "Special section guest editorial: tissue polarimetry," *J. Biomed. Opt.* **7**, 278 (2002).
2. P. J. Wu and J. T. Walsh, Jr., "Stokes polarimetry imaging of rat tail tissue in a turbid medium: degree of linear polarization image maps using incident linearly polarized light," *J. Biomed. Opt.* **11**, 014031 (2006).
3. J. F. de Boer and T. E. Milner, "Review of polarization sensitive optical coherence tomography and Stokes vector determination," *J. Biomed. Opt.* **7**, 359–371 (2002).
4. D. J. Maitland and J. T. Walsh, Jr., "Quantitative measurements of linear birefringence during heating of native collagen," *Lasers Surg. Med.* **20**, 310–318 (1997).
5. J. F. de Boer, T. E. Milner, M. J. C. van Gemert, and J. S. Nelson, "Two-dimensional birefringence imaging in biological tissue by polarization-sensitive optical coherence Tomography," *Opt. Lett.* **22**, 934–936 (1997).
6. R. J. McNichols and G. L. Côté, "Optical glucose sensing in biological fluids: an overview," *J. Biomed. Opt.* **5**, 5–16 (2000).
7. X. Guo, M. F. G. Wood, and I. A. Vitkin, "Angular measurement of light scattered by turbid chiral media using linear Stokes polarimeter," *J. Biomed. Opt.* **11**, 041105 (2006).
8. Q. Wan, G. L. Coté, and J. B. Dixon, "Dual-wavelength polarimetry for monitoring glucose in the presence of varying birefringence," *J. Biomed. Opt.* **10**, 024029 (2005).
9. D. Côté and I. A. Vitkin, "Balanced detection for low-noise precision polarimetric measurements of optically active, multiply scattering tissue phantoms," *J. Biomed. Opt.* **9**, 213–220 (2004).
10. R. R. Ansari, S. Bockle, and L. Rovati, "New optical scheme for a polarimetric-based glucose sensor," *J. Biomed. Opt.* **9**, 103–115 (2004).
11. K. C. Hadley and I. A. Vitkin, "Optical rotation and linear and circular depolarization rates in diffusively scattered light from chiral, racimic and achiral turbid media," *J. Biomed. Opt.* **7**, 291–299 (2002).
12. I. A. Vitkin, R. D. Laszlo, and C. L. Whyman, "Effects of molecular asymmetry of optically active molecules on the polarization properties of multiply scattered light," *Opt. Express* **10**, 222–229 (2002).
13. K. V. Larin, M. Motamedi, M. S. Eledrisi, and R. O. Esenaliev, "Noninvasive blood glucose monitoring with optical coherence tomography," *Diabetes Care* **25**, 2263–2267 (2002).
14. I. A. Vitkin and E. Hoskinson, "Polarization studies in multiply scattering chiral media," *Opt. Eng.* **39**, 353–362 (2000).
15. M. P. Silverman, W. Strange, J. Badoz, and I. A. Vitkin, "Enhanced optical rotation and diminished depolarization in diffusive scattering from a chiral liquid," *Opt. Commun.* **132**, 410–416 (1996).
16. B. D. Cameron and G. L. Côté, "Noninvasive glucose sensing utilizing a digital closed loop polarimetric approach," *IEEE Trans. Biomed. Eng.* **44**, 1221–1227 (1997).
17. J. C. Ramella-Roman, K. Lee, S. A. Prahl, and S. L. Jacques, "Design, testing, and clinical studies of a handheld polarized light camera," *J. Biomed. Opt.* **9**, 1305–1310 (2004).
18. S. L. Jacques, R. J. Roman, and K. Lee, "Imaging skin pathology with polarized light," *J. Biomed. Opt.* **7**, 329–340 (2002).
19. S. P. Morgan and I. M. Stockford, "Surface-reflection elimination in polarization imaging of superficial tissue," *Opt. Lett.* **28**, 114–116 (2003).
20. S. G. Demos, H. B. Radousky, and R. R. Alfano, "Deep subsurface imaging in tissues using spectral and polarization filtering," *Opt. Express* **7**, 23–28 (2000).
21. J. M. Schmitt, A. H. Gandjbakhche, and R. F. Bonner, "Use of polarized light to discriminate short path photons in a multiply scattering medium," *Appl. Opt.* **31**, 6535–6546 (1992).
22. V. Sankaran, J. T. Walsh, Jr., and D. J. Maitland, "Comparative study of polarized light propagation in biological tissues," *J. Biomed. Opt.* **7**, 300–306 (2002).
23. A. D. Kim and M. Moscoso, "Influence of the refractive index on the depolarization of multiply scattered waves," *Phys. Rev. E* **64**, 026612 (2001).
24. N. Ghosh, H. S. Patel, and P. K. Gupta, "Depolarization of light in tissue phantoms—effect of a distribution in the size of scatterers," *Opt. Express* **11**, 2198–2205 (2003).
25. D. Bicout, C. Brosseau, A. S. Martinez, and J. M. Schmitt "Depolarization of multiply scattered waves by spherical diffusers: influence of size parameter," *Phys. Rev. E* **49**, 1767–1770 (1994).
26. I. A. Vitkin and R. C. N. Studinski, "Polarization preservation in diffusive scattering from in-vivo turbid biological media: effects of tissue optical absorption in the exact backscattering direction," *Opt. Commun.* **190**, 37–43 (2001).
27. D. Côté and I. A. Vitkin, "Robust concentration determination of optically active molecules in turbid media with validated three-dimensional polarization sensitive Monte Carlo calculations," *Opt. Express* **13**, 148–163 (2005).
28. R. A. Chipman, "Polarimetry," Chap. 22 in *Handbook of Optics*, 2nd ed., M. Bass, Ed., Vol. **2**, pp. 22.1–22.37, McGraw-Hill, New York (1994).
29. C. Brosseau, *Fundamentals of Polarized Light: A Statistical Optics Approach*, Wiley, New York (1998).
30. S. Yau Lu and R. A. Chipman, "Interpretation of Mueller matrices based on polar decomposition," *J. Opt. Soc. Am. A* **13**, 1106–1113 (1996).
31. S. Manhas, M. K. Swami, P. Buddhiwant, N. Ghosh, P. K. Gupta, and K. Singh, "Mueller matrix approach for determination of optical rotation in chiral turbid media in backscattering geometry," *Opt. Express* **14**, 190–202 (2006).
32. M. F. G. Wood, X. Guo, and I. A. Vitkin, "Polarized light propagation

in multiply scattering media exhibiting both linear birefringence and optical activity: Monte Carlo model and experimental methodology," *J. Biomed. Opt.* **12**, 014029 (2007).

33. A. Suroweic, "PA Gel 915 MHz muscle-equivalent phantom material," *Int. J. Hyperthermia* **8**, 795–801 (1994).

34. C. F. Bohren and D. R. Huffman, *Absorption and Scattering of Light by Small Particles*, Chap. 2, Wiley, New York (1983).

35. D. Côté and I. A. Vitkin, "Pol-MC: a three dimensional polarization sensitive Monte Carlo implementation for light propagation in tissue," available online at http://www.novajo. ca/ont-canc-instbiophotonics/.

36. L. Wang, S. L. Jacques, and L. Zheng, "MCML—Monte Carlo modeling of light transport in multi-layered tissues," *Comput. Methods Programs Biomed.* **47**, 131–146 (1995).

37. R. Clark Jones, "New calculus for the treatment of optical systems VII. Properties of the N-matrices," *J. Opt. Soc. Am.* **38**, 671–685 (1948).

38. D. S. Kliger, J. W. Lewis and C. E. Randall, *Polarized Light in Optics and Spectroscopy*, Chap. 5, Academic Press–Harcourt Brace Jovanovich, New York (1990).

39. J. Morio and F. Goudail, "Influence of the order of diattenuator, retarder, and polarizer in polar decomposition of Mueller matrices," *Opt. Lett.* **29**, 2234–2236 (2004).

40. I. S. Sokolnikoff, *Mathematical Theory of Elasticity*, Krieger, Malabar, Florida (1983).

41. M. K. Swami, S. Manhas, P. Buddhiwant, N. Ghosh, A. Uppal, and P. K. Gupta, "Polar decomposition of 3×3 Mueller matrix: a tool for quantitative tissue polarimetry," *Opt. Express* **14**, 9324–9337 (2006).

42. X. Guo, M. F. G. Wood, and I. A. Vitkin, "Monte Carlo study of path length distribution of polarized light in turbid media," *Opt. Express* **15**, 1348–1360 (2007).

43. X. Guo, M. F. G. Wood, and I. A. Vikin, "A Monte Carlo study of penetration depth and sampling volume of polarized light in turbid media," *Opt. Commun.* **281**, 380–387 (2008).